# Micro-Rheometer

Joanna Zemla, Claude Verdier, Yara Abidine

# 5.1 (Micro-)Rheometer

*Joanna Zemła, Institute of Nuclear Physics Polish Academy of Sciences, Krakow, Poland*
*Claude Verdier, University Grenoble Alpes, CNRS, LIPhy, Grenoble, France*
*Yara Abidine, University Grenoble Alpes, CNRS, LIPhy, Grenoble, France*

To exchange

## 5.1.1 Oscillatory rheology

When oscillatory strain γ deformation with amplitude $\gamma_0$ and angular frequency ω (ω= 2πf) is applied, the stress σ will oscillate in time (t) but its oscillations will be phase shifted by φ.

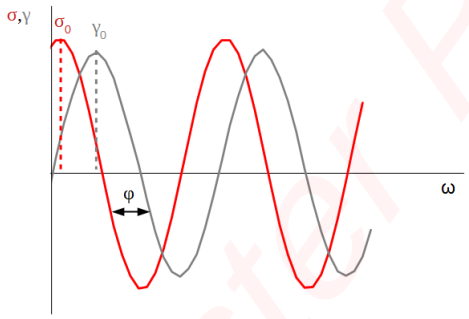


omega should be time (t)
phi should be phi/omega

***Figure 1**: Stress σ and strain γ time evolution in oscillatory measurements. Stress and strain are shifted by angle φ. Stress and strain amplitudes are labeled with $\sigma_0$ and $\gamma_0$, respectively.*

$$\gamma(t)=\gamma_0 \sin \omega t \quad (1a)$$

$$\sigma(t)=\sigma_0 \sin(\omega t+\varphi) \quad (1b)$$

The phase shift is always between 0° and 90°. In case of ideally elastic materials the phase shift is 0°, while ideally viscous samples reveal φ= 90°. Materials with phase shift in between these values are viscoelastic and their stress is expressed as a sum of storage modulus G' and loss modulus G'', parameters reflecting elastic and viscous properties of the sample, respectively.

$$\sigma(t)=\gamma_0(G'' \cos \omega t+G' \sin \omega t) \quad (2)$$

These relations show that stress σ is proportional to strain or strain amplitude, which is true for all material types at low strains and is called the linear viscoelastic range (LVER). Thus, at the LVER range G' and G'' are independent of stress or strain amplitudes. Usually, one has to perform a strain sweep in order to determine under which deformation ($\gamma_0$) moduli G' and G'' remain constant, i.e. are in the LVER.

## 5.1.2 AFM- based oscillatory microrheology

### 5.1.2.1 Microrheological measurements

Rheological measurements were performed with atomic force microscope, Nanowizard II (JPK, Berlin, Germany) working in force modulation mode. The AFM system was integrated with

inverted optical microscope Observer D1 (Carl Zeiss, Jena, Germany). Cells were measured in non-supplemented medium at 37 $^0$C, with silicon nitride MLCT cantilevers (Bruker, Germany). The MLCT (probe C) is a four sided pyramid with nominal spring constant k~0.01 N/m that was calibrated using the thermal noise method (Butt and Jaschke 1995). The loading operating force (200 pN) corresponded to an initial indentation depth $\delta_0$ lower than 1 μm. The relationship between the force and indentation depth is described with Hertz- Sneddon contact mechanics model (Sneddon 1965):

$$F = \frac{3E\tan\theta}{4(1-\nu^2)}\delta^2 \quad (3),$$

where E is the cell's Young's modulus, ν is the Poisson's ratio, which for incompressible cells is roughly 0.5, and θ~20 deg is the front half opening angle of the probing tip. When the low amplitude oscillations at initial indentation depth $\delta_0$ are superposed then the complex shear modulus $G^*(\omega)$ can be determined (Alcaraz *et al*, 2003) using the formula

$$G*(\omega) = \frac{1-\nu}{3\,\delta_0\tan\theta}\frac{F*(\omega)}{\delta*(\omega)} \quad (4),$$

where F*(ω) and δ*(ω) are the Fourier transforms of measured force and sample indentation depth, respectively, ω= 2πf is the angular frequency, and f is the frequency in Hz (Alcaraz *et al*, 2003; Abidine *et al*, 2015a, 2015b, 2018).

In addition, the complex shear modulus G*(ω) = G'(ω) + i G''(ω), where G'(ω) is the storage modulus- a measure of the elastic energy stored and recovered per cycle of oscillations, and G''(ω) is so called loss modulus- a measure of the energy dissipated per cycle of sinusoidal oscillations. The ratio of G''(ω) and G'(ω) equals tan φ, a parameter also called the loss factor. If tan φ << 1, a solid like behavior of the sample is assumed, and if loss factor >> 1, a Newtonian fluid behavior is assumed.

5.1.2.2 Microrheological models

Rheological models have been studied for years in the polymer community, since polymers can be subjected to shear deformations at very different frequencies which are important in the industry (rubbers, plastics, pastes, foods, foams, etc.). The basic models are the Maxwell and Voigt models (Verdier *et al*, 2009) which can be used in series or parallel. Such models contain different relaxation times, that can be used in association (Maxwell modes):

tau_i

$$G' = \sum_{i=1}^{N} G_i \frac{\omega^2\tau_i^2}{1+\omega^2\tau_i^2}, G'' = \sum_{i=1}^{N} G_i \frac{\omega\tau_i}{1+\omega^2\tau_i^2} \quad (5)$$

where $t_i$ is a relaxation time, and $G_i$ the corresponding modulus.

These relations are quite useful but appear to be insufficient to describe a more complex rheology. Therefore integral models (Baumgartel *et al*, 1990) or fractal ones (Palade *et al*, 1996, Abdine *et al*, 2015b) have been used instead. These models are quite efficient for describing the whole range covering several decades in frequency f (Hz). More recently, Sollich *et al*. 1997 proposed an elegant model based on structural disorder and metastability, after introducing a mean field temperature and proper statistical treatment. They were able to find various behaviors (yield stress, shear thinning, glassy behavior) that encompass most of the rheology of soft materials, including cells and tissues. This model has been successfully used for describing adherent cell behaviors (Bursac *et al*, 2005).

Although complex, these models often seem to predict generic power law behaviors (Alcaraz *et al*, 2003, Abidine *et al*, 2015a, 2018) in a certain range of frequencies, therefore it is sometimes useful

to replace them with an easier model with less parameters to explain the dynamic behavior of moduli G' and G''. This will be shown in §5.2.2 for cancer cells microrheology. The model parameters that are found can be used for describing cells or cell behavior. In particular, it was shown recently that cancer cells in a glassy state can remodel their actin microstructure quite rapidly in order to transmigrate through the endothelium during cancer metastasis (Abidine *et al,* 2018). Therefore the present techniques can become quite efficient for predicting different behaviors, i.e. normal vs. sick cells and constitute a new powerful tool for characterizing/differentiating cells *in vitro*.

Finally, viscoelastic behaviors are one type of classical behavior at low deformation but more recent studies show that visco-elasto-plastic or poro-elastic behaviors can also be encountered for cells (Moeendarbary *et al,* 2013) and tissues (Preziosi *et al,* 2010).

### 5.1.3 Oscillatory shear macrorheology

The basic oscillatory macrorheological experiments are called 'frequency sweep' and 'strain/stress amplitude sweep'. During frequency sweep experiment, the G' and G'' evolutions as a function of frequency are observed. This type of measurement gives information about the (micro)structure and dynamics of the system. Strain sweeps are oscillatory measurements at fixed frequency with increasing strain amplitude. In this approach a linear viscoelastic range should be observed at low strain amplitudes (see §5.1.1). For most gel samples at higher strain values the G' and G'' will depend on the strain amplitude. Higher values of G' will be observed at low strains, while at high stress amplitudes, G'' may exceed the storage modulus G'. This larger G'' reflects the breakage of the gel structure. Out of the LVER, storage and loss moduli are not well defined as the strain signals will not be sine functions, as they may contain different frequencies (Preziosi *et al,* 2010). However, Storm *et al.* (Storm *et al.* 2005) have shown, for highly nonlinear material, that the error made in estimating the moduli by fitting such data using a sine function can be small.

Macro- rheological experiments were performed using a parallel plate rotational rheometer MRC302 (Anton Paar, Graz, Austria) at 22$^{o}$C with a plate diameter of 4 mm and a torque limit 200 mNm. Measurements were conducted on muscle tissue samples ~1 mm thickness. The slices were placed between the plates and environmental chamber was closed. Amplitude sweeps were conducted at frequency of 1 rad/s and shear range of 0.01-1%. To avoid sample slippage 20% preload (compressive strain) has been applied. Storage G' and loss G'' moduli values were calculated using the Anton Paar software.

### 5.1.4 Cells and tissue samples

Benign cancer of ureter cell line (HCV 29), and four malignant cancer cell lines of different grades (RT112, G2; 5637, G2; T24, G2-3 and J82, G3) were examined. The cells were cultured in RPMI 1640 medium supplemented with 10% fetal calf serum (FBS) at 37$^{o}$C in a humidified 5% $CO_2$ atmosphere. Cells were seeded on plastic (TPP Petri dishes, Switzerland) or glass substrates covered with FN with cell density allowing measurements of isolated cells after 24h and 48h of growth.

Tibialis antherior (TA) muscles were explanted from wild-type B6 SCID mice and mdxSCID (mouse model for studying Duchenne's Muscular Distrophy) during experiments on cell-

transplantation based treatment (Iyer *et al.* 2018). TA samples were placed in tubes containing DMEM (Dulbecco's modified Eagle medium) admixed with 10% DMSO (dimethyl sulfoxide) and stored in liquid nitrogen for additional experiments. Prior to the measurements, samples were defreezed to room temperature and subsequently cut using lancet and biopsy punch to obtain tissue samples of 1 mm in thickness and 4 mm in diameter. The samples were cut along the muscle fibers.

### 5.2.1 AFM-based characterization of cell viscoelastic properties

Rheology studies how materials deform in time under an applied external force. Information on the viscous properties of the material can be provided by applying small amplitude oscillatory strains or stresses to the sample. When oscillatory strain deformation is applied, the stress will also oscillate in time t but its oscillations will be phase shifted.

Shroff *et al.* (Shroff *et al*, 1995) were the first to use an oscillating AFM probe to study the mechanical properties of rat atrial myocytes. They investigated cell mechanical changes during a single contraction, and found a dynamic increase of cell stiffness proportional to its contraction. It has also been shown that environmental conditions (substrate rigidity, $Ca^{2+}$ ions concentration, fixation) result in growth of the elasticity parameter. This approach was further developed by Alcaraz *et al.*(Alcaraz *et al,* 2003). The method they have introduced allows determination of the complex shear modulus G*(ω) from oscillatory measurements over a chosen frequency range (see §5.1.2.1). What is important is that the method takes into account the probe-cell contact geometry as well as the viscous drag corrections in the microrheological model. Alcaraz *et al.* (Alcaraz *et al*, 2003) studied the microrheological properties of alveolar (A549) and lung epithelial cells (BEAS-2B) in the frequency range [0.1Hz- 100 Hz]. They showed that both G' and G'' change with frequency and that the rheology of lung epithelial cells resembles the one of soft glassy materials close to a glass transition, and assumed that structural disorder and metastability may be fundamental features of cell organization (Alcaraz *et al,* 2003).

### 5.2.2 Bladder cancer cell lines viscoelastic characteristics

The AFM-based microrheological technique was also applied to study viscoelastic properties of T24 bladder cancer cells (Abidine *et al*, 2015a, 2018). Measurements performed at different locations on the cell (over nucleus, at perinucleus, and at the edge) showed that there exists a varying plateau elastic modulus, depending on cell location: cell stiffens away from its nucleus (Fig. 2 and 4A-C), thus, $G_N^0$ (nucleus)< $G_N^0$ (perinucleus)< $G_N^0$ (edge) (Abidine *et al,* 2015a), which is in agreement with the conclusions of Shroff *et al.* (Shroff *et al,* 1995).

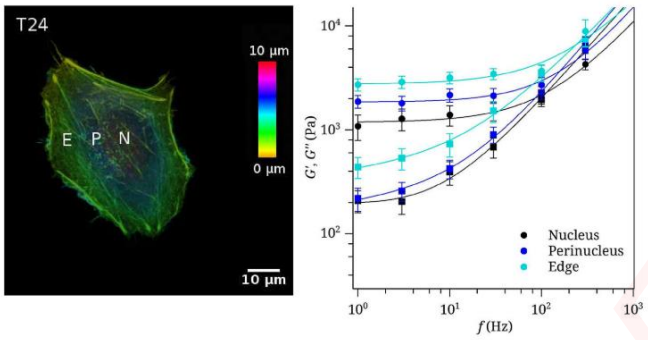


***Figure 2**: Left: Confocal images of a single T24 cell. A z-projection with a color scale corresponding to the height (yellow is the basal side of the cell, and red is on top of the cell). Indentations are made at three locations: nucleus (N), perinucleus (P) and edge (E). The cells are in a low migrating state. Right: Evolution of moduli G' (circle) and G'' (square) on the nucleus (black), perinucleus (blue) and edge of the cell (cyan); N = 20 and error bars represent SEM. Curves were fitted with the model. (Reprinted with permission from Abidine et al. 2015a)*

Additionally, the mechanical properties of bladder cancer cell lines of different malignancy have been compared, RT112, T24 and J82 bladder cancer cell lines, ordered by increasing malignant potential (Abidine *et al*, 2015a, 2018). The results indicate that |G*| decreases with invasiveness and cells become glassy (decrease of transition frequency $f_T$, being the crossover of G' and G''), which was shown by a decrease of storage modulus values obtained for RT112, T24 and J82 bladder cancer cell lines (Fig. 3). This research also showed that viscoelastic properties of cells strongly depend on cytoskeleton organization. Bladder cancer cells treated with Latranculin A, a drug causing depolymerization of actin fibers, revealed a decrease of storage modulus at low frequencies (Abidine *et al*, 2015a). It has also been investigated whether substrate rigidity modifies the nanomechanical characteristics of cells. T24 cells were grown on polyacrylamide gels of rigidity of 5, 8 and 28 kPa (Fig. 4) and an increase of $|G^*|$ was observed, showing a clear mechanosensitivity effect. It has already been reported that measurements of mechanical properties of cells grown on rigid substrates may result in overestimated Young Modulus (E) values, interestingly, data presented in Abidine *et al.* 2018 indicates that the elastic modulus E obtained for cells grown on soft substrates may result in an underestimation of E. This assumption is illustrated by comparison of $G^*$ and $G^*_{cor}$ data obtained for bladder cancer lines, where $|G^*|$ is the modulus calculated from Eq. (4) above and $|G^*_{cor}|$ from Eq. (5) in (Abidine *et al*, 2018).

Latrunculin

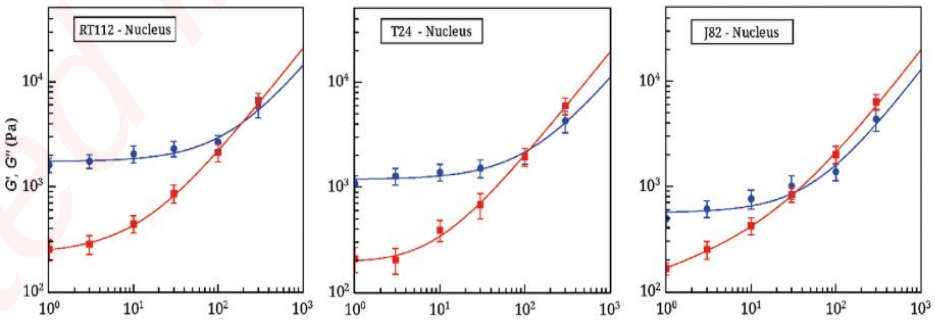


***Figure 3**: Evolution of G' (blue circle) and G'' (red square) on the nucleus (N) of three cancer cell lines: RT112, T24 and J82 (left to right, respectively, N = 10, N = 20, N = 10, error bars represent mean± SEM). Reprinted with permission from (Abidine et al. 2015a).*

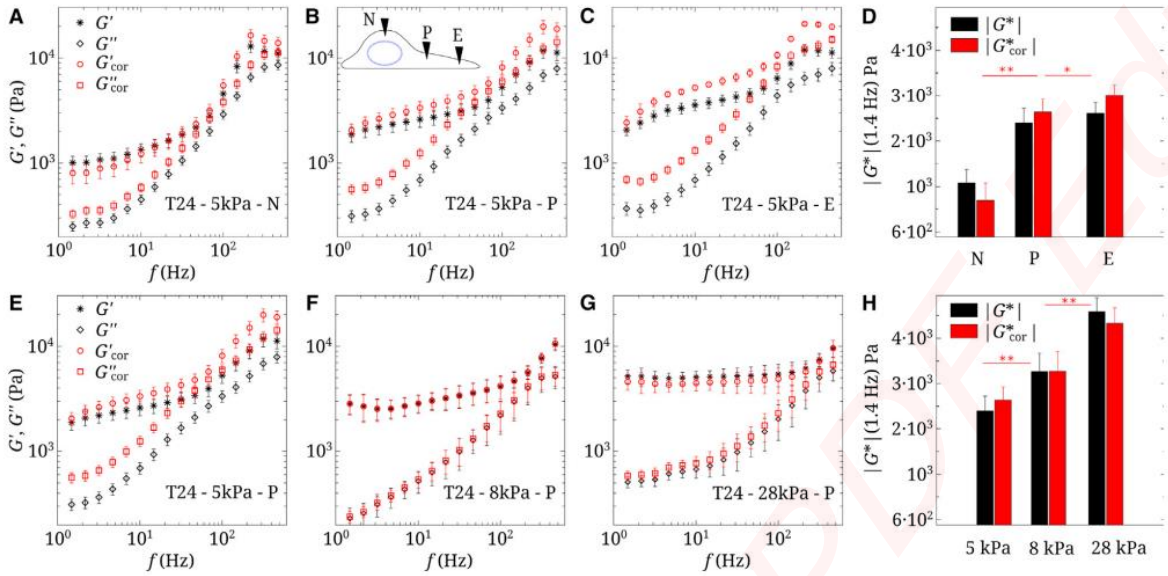


***Figure 4**: Raw and corrected viscoelastic moduli of T24 cells. (A–C) Data on a 5 kPa gel at three locations (nucleus (N), perinuclear region (P), and edge (E)) are shown. (D) Modulus $|G^*|$ (1.4 Hz) at the three locations (N, P, and E) is shown. (E–G) Data measured in the perinuclear region (P) of cells on three gels ($E_2$ = 5, 8, and 28 kPa). n = 5, and error bars represent the mean ± SE. (H) Modulus $|G^*|$ (1.4 Hz) for the three gels are shown ($E_2$ = 5, 8, and 28 kPa). Statistical relevance is shown for corrected values of $|G^*|$. Reprinted with permission from (Abidine et al. 2018)*

Studies on characterization of viscoelastic properties of bladder cancer cell lines have been continued using non-malignant ureter cancer, HCV 29, and 5637 bladder cancer cell lines. The T24 cell line was also investigated as a reference allowing to compare the obtained results with data presented by Abidine *et al.* 2015. The measurements were performed using a similar setup and protocol as described in §5.1.2.1 over cell nuclei after 48h of cell growth. The data have been fitted using a simplified model, where the cell elastic and viscous moduli are described with the following equations:

$$G'(\omega) = G_N^0 + k_1 \omega^a \quad (6a)$$

$$G''(\omega) = k_0 + b k_1 \omega^a \quad (6b)$$

With this approach, the angular transition frequency $\omega_T$ corresponding to the crossing of G' and G'' can be simply calculated from solving the equation G'= G'', which gives (since b>1):

$$\omega_T = \left(\frac{G_N^0 - k_0}{k_1 (b-1)}\right)^{(1/a)} . \quad (7)$$

The evolution of G' and G'' as a function of angular frequency is presented in Figs 5D-F. The plateau modulus values obtained for the T24 cell line are in agreement with data published in Abidine *et al.* 2015 (compare Fig. 3 and 5). We find that benign cells are stiffer than the cancerous ones, as expected.

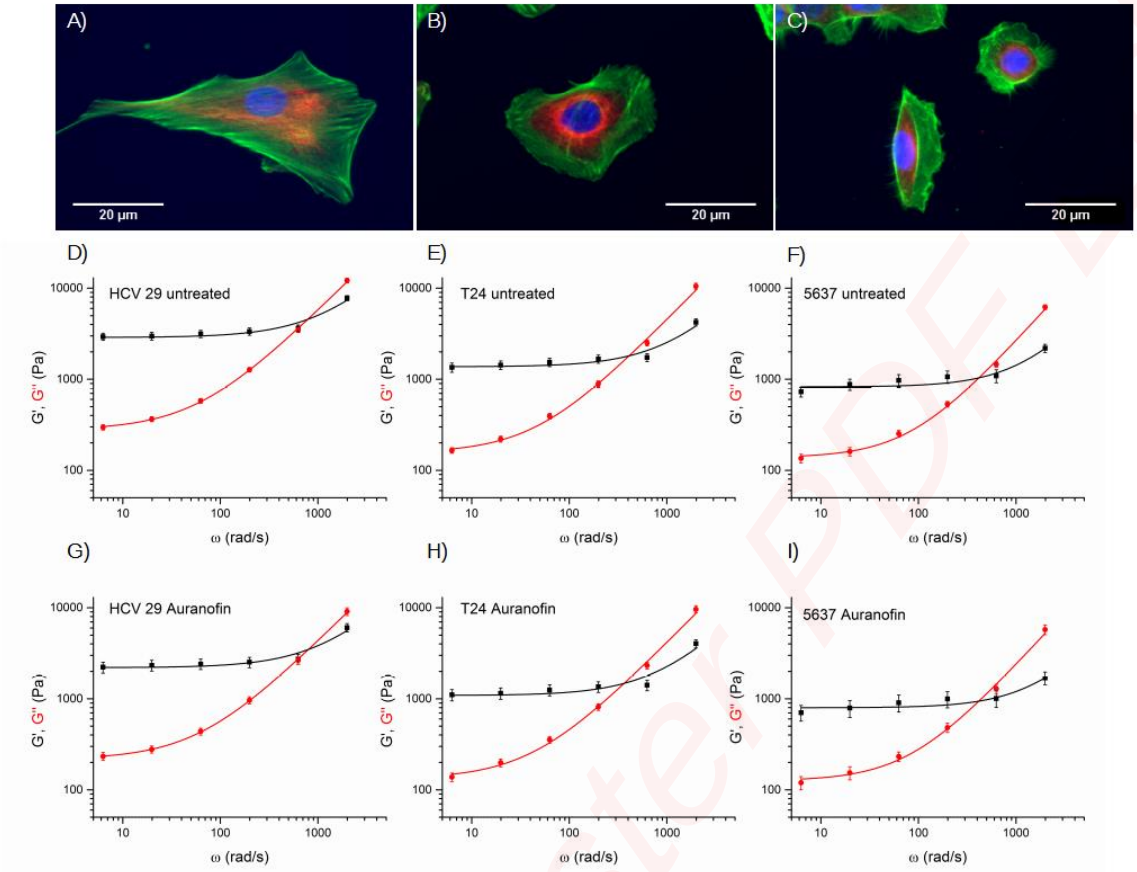


***Figure 5:*** *Cytoskeleton structure of HCV 29, T24 and 5637 cell lines imaged with fluorescence microscopy. Actin filaments are stained in green, microtubules are in red and nuclei in blue (A-C). G' (black) and G'' (red) of untreated (D-F) and Auranofin treated (G-I) bladder cancer cell lines. Data are presented as mean±SEM. N(untreated)= 72 (HCV 29), 58 (T24), 31 (5637) and N(Auranofin)= 44 (HCV 29), 46 (T24), 24 (5637).*

Additionally, the plateau modulus of the 5637 cell line is lower than both HCV 29 and T24 cell lines (Fig. 6). This effect may result from their cytoskeleton structure, which is more complex in the case of HCV 29 cells (Fig. 5A-C). Fluorescent staining reveals stress fibers in HCV 29 as well as in T24 cell lines. The cytoskeleton of 5637 cells is very poorly developed. They seem to be unable to develop either stress fibers or microtubules. The obtained results allow to assume that the cytoskeleton structure is closely linked to the cell mechanical properties.

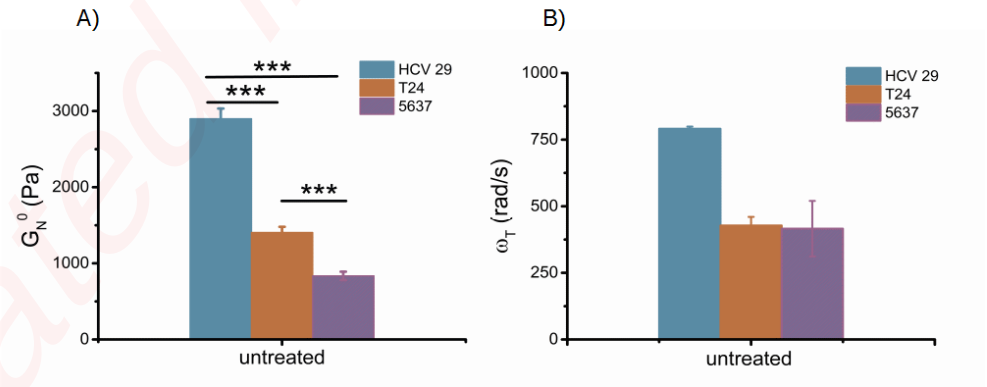


***Figure 6****: Mean values of plateau modulus $G_N^0$ (A) and transition angular frequency $\omega_T$ (B) obtained for non-malignant (HCV 29), and cancer cell lines (5637, G2 and T24, G2-3). The error bars are SEM and statistical analysis was performed with a two-sample unpaired Student's t-test (*** refer to p< 0.001). N= 72 (HCV 29), 58 (T24), 31 (5637).*

It has been concluded that in the case of bladder cancer cell lines, changes of cell rigidity are correlated with their invasive potential (Abidine *et al*, 2015a, 2018). In Fig. 6 plateau modulus mean values as well as transition angular frequency mean values calculated for the above mentioned bladder cancer cell lines are compared. The micro- rheological properties of the benign cell line are characterized by the highest values of $G_N^0$ and $\omega_T$, which is in agreement with the previous conclusions. Yet, investigation of Fig. 6B reveals no difference (within error bars) between $\omega_T$ values obtained for T24, grade 2-3, and 5637, grade 2, cancer cell lines. These results may indicate that plateau modulus values are determined by cytoskeleton structure, and the transition frequency is the parameter strongly correlated with cell invasiveness, i.e. its ability to remodel the cytoskeleton rapidly or not.

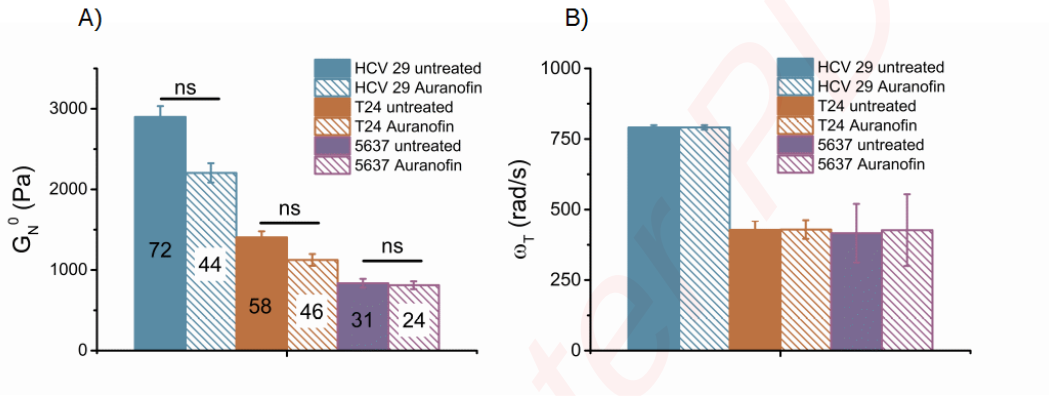


***Figure 7**: Comparison of microrheological model parameters calculated for HCV 29, T24 and 5637 cell lines treated with Auranofin. $G_N^0$ and $\omega_T$ values obtained for reference samples are plotted as well. The error bars are SEM and statistical analysis was performed with a two-sample unpaired Student's t-test (p> 0.05 refers to no statistical significance, ns). In bars the amounts of measured cells are indicated.*

2015a

It has already been shown that exposing cells to chemicals modifying their cytoskeleton structure results in changes of microrheological properties (Abidine *et al*, 2015b). However, the intriguing question was if other types of anticancer drugs modify the cell's viscoelastic properties as well. HCV 29, T24 and 5637 bladder cancer cell lines were exposed for 72h to Auranofin, AF, a chemical causing hyperoxidation via mitochondria deregulation. A relatively low dose of 0.2μM was used. The concentration was chosen basing on cell proliferation tests (MTS, Sigma Aldrich) performed at AF concentrations of 0.01, 0.1, 1.0 and 10μM. The results were normalized to control samples and no drug effect on bladder cells proliferation was observed at concentrations of 0.01 and 0.1μM. 1.0μM AF did not affect HCV 29 proliferation while the number of T24 cells decreased by 30% and 5637 cells by 75%. The results indicate that cells respond to 0.2μM AF by changes in proliferation rate.

Before the microrheological measurements, the drug-containing medium was replaced with supplemented RPMI 1640 medium. The cells were indented on top of their nuclei. The G' and G'' values were calculated using Eq. (4). The data presented in Fig. 5 and 7 show that this dose of AF has not influenced the mechanical properties of studied cells, which may result from either too low AF concentration or the fact that this chemical does not target cytoskeleton structures directly.

### 5.2.3 Model tissue viscoelastic properties

We first start to study model tissues. Such tissues contain ExtraCellular Matrix (ECM) and cells. They can be tested using classical rheology using a plate-plate rheometer (Iordan *et al*, 2010). This geometry is preferred in this case since it allows to compress the biological tissue into the rheometer without including too much pres-stress through normal forces. Several studies are discussed, where the concentration of the collagen is varied and where the cell concentration is also changed. In our study, we used CHO cells (Chinese Hamster Ovary). Considering the collagen only, we find that the collagen network without cells is viscoelastic, as expected, with a slightly higher elastic modulus G' as compared to the loss modulus G'' (see Fig. 8 below)

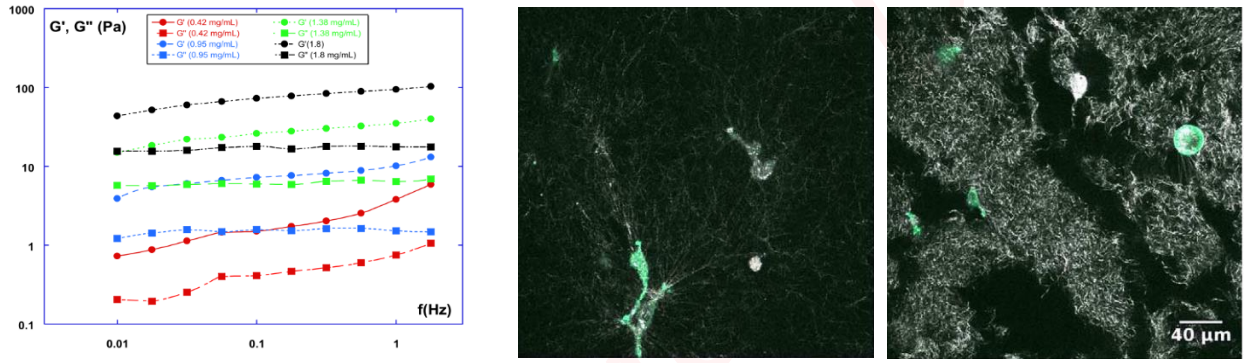


***Figure 8****: Left: Viscoelastic properties of collagen networks (G' and G") as a function of collagen concentration, from 0.42 mg/mL until 1.8 mg/mL. Centre and right: CHO cells embedded in collagen matrix (center 0.42 mg/mL and right, 1.8 mg/mL). Reprinted from (Iordan et al. 2010)*

The plateau modulus $G_N^0$ can be obtained at the lowest frequency (0.01Hz) and plotted in terms of the collagen concentration c and leads to a relationship of the kind $G_N^0 \sim c^{2.6}$, in agreement with the work of Vader *et al.* 2009. Note that the LVER lies below 5% strain in such gels.

Now we insert cells into the matrix (collagen network) and the results show again viscoelastic effects (Iordan *et al*, 2010). The amount of CHO cells that were included goes up to 1.8 $10^7$ cells/mL. There is an elasticity increase as cells are inserted into the gel (for example at 0.95 mg/mL G' increases from 3 Pa to 8 Pa) but at collagen concentrations higher than 0.95 mg/mL, the inverse is observed and the elasticity decreases (for example from 50 Pa down to 10 Pa for the 1.8mg/mL collagen concentration). Plotting again $G_N^0$ as a function of c leads to a smaller slope $G_N^0 \sim c^1$, raising the question of what governs such a dependence.

Obviously interactions between cells and the matrix take place, which can be followed thanks to confocal reflectance microscopy (Friedl *et al*, 2001). Figure 8 shows typical CHO cells embedded in two different collagen matrices (0.42 and 1.8mg/mL). Their behavior changes as there is enough space at low collagen concentration to migrate and adhere to the fibres, therefore they are more elongated. On the other hand, at higher concentrations, they remain round as there is no space. It was also shown that cells attract collagen as they move slowly into the matrix and carry it along, leaving holes or tunnels behind (see last photograph on the right). We conclude that the interplay between collagen fibres and cells has two opposite effects: Figure

a) cells in low density networks have space, and elongate, pull on fibres, modifying the collagen structure therefore its rheology

b) cells in high density matrix have no space so they interact more with collagen to remodel it. They can attract it, and therefore can dig tunnels through it. Therefore the collagen structure breaks down

and the relationship between the plateau modulus $G_N^0$ and the concentration shows a much smaller slope at the high concentrations.

To conclude, ECM interactions with cells are complex and need be taken into account for proper understanding/modeling of tissues. Classical hyperelasticity laws for tissues can be used but they need to be refined, taking into account cell-cell and cell-ECM interactions in order to be more accurate, as proposed in recent works (Preziosi *et al*, 2010).

### 5.2.4 Brain, liver and kidney tissues macrorheological properties

It is a known fact that many pathological reactions such as cancer (Caroline *et al*, 2014), liver and kidney fibrosis (Desmoulière *et al*, 2003), respiratory system diseases (Zemła *et al*, 2018b) or Duchenne muscular dystrophy (DMD) (Puttini *et al*, 2009; van Zwieten *et al*, 2014) manifest themselves by tissue/ ECM remodeling. The remodeling results in changes of mechanical properties of tissues, which was revealed by Young's modulus determination (AFM measurements) of diseased (diseased and healthy) brain (Ciasca *et al*, 2016), breast (Plodinec *et al*, 2012; Ansardamavandi *et al*, 2016), liver (Tian *et al*, 2015), and cervical cancer biopsies (Cui *et al*, 2017), or asthmatic (Zemła *et al*, 2018b) and DMD (van Zwieten *et al*, 2014; Iyer *et al*, 2018) tissue samples, and also shown above in model tissues (§5.2.3). At microscale AFM measurements of tissue samples allow to distinguish between the pathological and normal tissue samples, although, the complexity of the tissue structure results in wide E distributions (Ansardamavandi *et al*, 2016; Zemła *et al*, 2018b) and, in some cases, in the multimodal distributions of E (Tian *et al*, 2015; Iyer *et al*, 2018). This, however, does not discriminate AFM as a tool to study mechanical properties of tissues but it seems that the complexity of the system may require a different method to reveal their viscoelastic properties, such as macrorheological measurements.

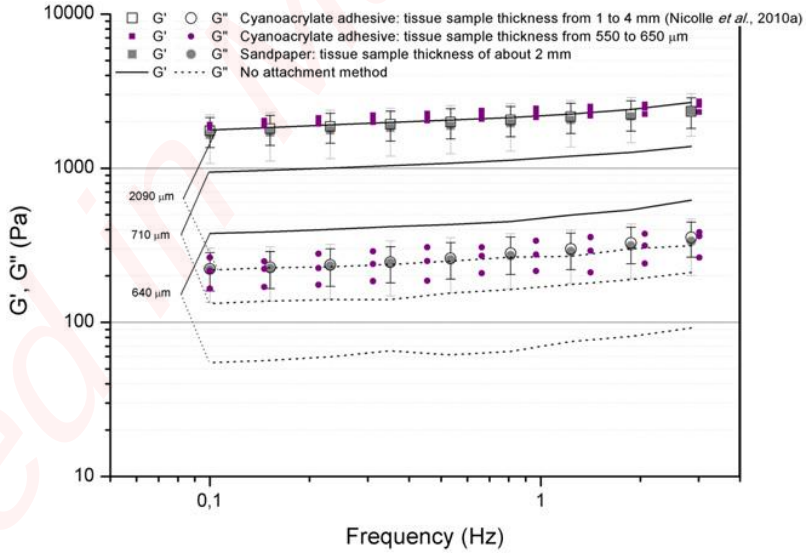


***Figure 9**: Storage (G') and loss (G") moduli of porcine kidney tissue according to frequency measured at small strains (0.1%) by using two sample attachment methods: glue and sandpaper. For comparison, the results from three glued thin samples (1 mm) and three unbound samples of different thickness are also plotted. Reprinted with permission from (Nicolle and Palierne 2012).*

First studies of macro- rheological properties of biological samples were performed for brain tissue samples (Bilston *et al*, 1997; Bilston 2003; Nicolle and Palierne 2012; Mao *et al*, 2012; Pogoda *et al*, 2014; Mihai *et al*, 2015; Qing *et al*, 2019), and liver (Tan *et al*, 2013; Perepelyuk *et al*, 2016). The above mentioned oscillatory shear measurements revealed a narrow LVER range of tissue samples at low strains (below 1%). Additionally, the issue of sample immobilization was also discussed. There are three common approaches: (1) no modification of plates, (2) gluing sand paper disks to rheometer plates and (3) gluing the sample with a cyanoacrylate adhesive to the plates. Nicolle and Palierne 2012 reviewed results obtained at these conditions and compared moduli values of porcine kidney tissue with respect to the tissue immobilization method (Fig. 9). They found no difference in storage and loss moduli for glue and sand paper immobilization type. The results, however, show that measurements performed without any additional tissue attachment resulted in decreased values of G' and G''. To avoid tissue sample slippage during oscillatory test, a preload, compressive strain exerted on a sample, may be applied (Tan *et al.* 2013). It has to be mentioned though, that measured G' and G'' moduli values depend on the preload. The higher compressive strain is applied the higher storage and loss moduli we get (Tan *et al*, 2013; Pogoda *et al*, 2014; Mihai *et al*, 2015). These results suggest that for comparative studies, the loss factor tan(φ) may be a good parameter as G'/G'' ratio does not depend on sample immobilization protocol (see Fig.9).

Recently, macrorheological measurements have been performed to compare viscoelastic properties of normal and scleris complex (TSC) brain tissue (Qing *et al*, 2019). TSC is a genetic disorder with a high penetrance of Autism Spectrum Disorders. Unfortunately, both AFM-nanomechanical characterization of the samples and macrorheological measurements did not exhibit differences between healthy and pathological tissue samples.

### 5.2.5 Duchenne muscular dystrophy macrorheological characteristics

Strain amplitude sweep tests (§5.1.3) were performed to characterize viscoelastic properties of normal and DMD tissue samples (Fig. 10A). The samples were prepared according to the procedure described in §5.1.4. Macro- rheological tests were performed at oscillations of 1 rad/s and at strain range of 0.01- 2%. To avoid sample slippage a preload (20%) sample compression was applied.

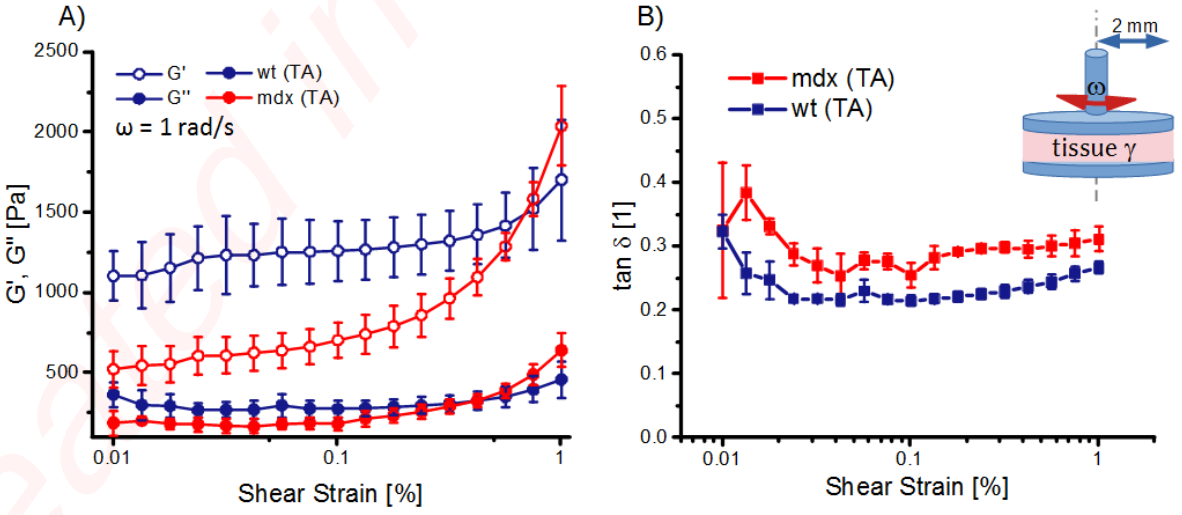

***Figure 10****: Comparison of storage (G') and loss (G'') modulus of normal (wt) and Duchenne dystrophy (mdx) mice tibialis arthritis (TA) muscles. (A) Loss factor calculated for wt and mdx tissues. In the inset the scheme of the rheometer is presented. (B) Data are mean± SEM, N= 5.*

Higher storage modulus values were obtained for wild type TA samples in comparison to mdx tissues (Fig. 10). We have observed an increase of the G' modulus with increasing shear strain. Interestingly, a similar behavior was shown for crosslinked biopolymer networks (Storm *et al.*, 2005). Indeed, TA muscle structure resembles that of a crosslinked network in a way, as it is built of aligned muscle fibers interconnected with collagen fibers present in endomysium, which envelopes each muscle fiber (Beunk *et al*, 2019). In Fig. 10B loss factor values calculated for both types of samples studied are plotted, and regardless of strain amplitude $G_{mdx}$'' to $G_{mdx}$' ratio is higher than $G_{wt}$'' to $G_{wt}$' ratio, which indicates that the storage modulus contributes less to the overall mechanical characteristics of mdx tissues as compared to wt tissues samples.

## Conclusions

Rheological tools, both at the micro- and macro-scales, are important tools to help understand the properties of cells and tissues. In any case, they cannot alone predict or elucidate all properties. When coupled with complementary observation techniques (classical and confocal microscopy, new super-resolution microscopy STED or STORM, ultrasound, X-rays, biology techniques), they allow to correlate the time-dependent microstructure of cells/tissues in order to understand the main mechanical features.

On the experimental side, there are many challenges to investigate the many different cell/tissue systems which still remain difficult to obtain, prepare, characterize according to well-defined protocols needing an impressive expertise. Probably this is the most important task that remains to be considered in the future, but it is very important, in particular since normal and unsane tissues definitely need to be characterized and compared.

From a theoretical point of view, it is still difficult nowadays to come up with rheological models containing both visco-elasto-plastic effects, the active nature of the cells and include their interactions between themselves and the extra-cellular matrix (ECM). The new challenge for the next decades will be to use the available models and enrich them with such properties.

**Acknowledgments**

*Joanna Zemła acknowledges the financial support of the French Government and the French Embassy in Poland.*

*Claude Verdier thanks the Nanoscience Foundation for financial support of the AFM, the LabeX Tec21 (Investissements d'Avenir, grant agreement No. ANR-11-LABX-0030) and the ANR "TRANSMIG" (grant No. 12-BS09-020-01).*

## Bibliography

Abidine, Y. Constantinescu, A. Laurent, V.,M. *et al.* (2018) "Mechanosensitivity of Cancer Cells in Contact with Soft Substrates Using AFM." Biophys J 114:1165–1175.

Abidine, Y. Laurent, V.,M. Michel, R. *et al.* (2013) "Microrheology of complex systems and living cells using AFM." Comput Methods Biomech Biomed Eng 16:15–16.

Abidine, Y. Laurent, V.,M. Michel, R. *et al.* (2015a) "Local mechanical properties of bladder cancer cells measured by AFM as a signature of metastatic potential." Eur Phys J Plus 130:202-215.

Abidine, Y. Laurent, V.,M. Michel, R. *et al.* (2015b) "Physical properties of polyacrylamide gels probed by AFM and rheology." EuroPhys Lett 109:38003-38008.

Alcaraz, J. Buscemi, L. Grabulosa, M. *et al.* (2003) "Microrheology of Human Lung Epithelial Cells Measured by Atomic Force Microscopy." Biophys J 84:2071-2079.

Ansardamavandi, A. Tafazzoli-Shadpour, M. Omidvar, R. Jahanzad, I. (2016) "Quantification of effects of cancer on elastic properties of breast tissue by Atomic Force Microscopy." J Mech Behav Biomed Mater. 60:234-242.

Beunk, L. Brown, K. Nagtegaal, I. *et al.* (2019) "Cancer invasion into musculature: Mechanics, molecules and implications." Semin Cell Dev Biol 93:36-45.

Bilston, L.,E. (2003) "Brain tissue properties at moderate strain rates" IMECE2003-4. In: American Society of Mechanical Engineers, Bioengineering Division (Publication) BED55:3–4.

Bilston, L.,E. Liu, Z. Phan-Thien, N. (1997) "Linear viscoelastic properties of bovine brain tissue in shear." Biorheology 34:377–385.

Bursac, P. Lenormand, G. Fabry, B. Oliver, M. Weitz, D.,A. Viasnoff, V. Butler. J.,P. and Fredberg, J.,J. (2005) "Cytoskeletal remodelling and slow dynamics in the living cell." Nat Mater, 4:557-561.

Butt, H.,J. and Jaschke, M. (1995) "Calculation of thermal noise in atomic force microscopy." Nanotechnology 6:1-7.

Caroline, B. Jonathan, C. Werb, Z. (2014) "Remodelling the extracellular matrix in development and disease." Nat Rev Mol Cell Biol 15:786–801.

Ciasca, G. Sassun, T.,E. Minelli, E. et al (2016) "Nano-mechanical signature of brain tumours." Nanoscale 8:19629–19643.

Cui, Y. Zhang, X. You, K. et al (2017) "Nanomechanical Characteristics of Cervical Cancer and Cervical Intraepithelial Neoplasia Revealed by Atomic Force Microscopy." Med Sci Monit 23:4205–4213.

Desmoulière, A. Darby, I.,A. Gabbiani, G. (2003) "Normal and Pathologic Soft Tissue Remodeling: Role of the Myofibroblast, with Special Emphasis on Liver and Kidney Fibrosis." Lab Investig 83:1689–1707.

Florea, C. Tanska, P. Mononen, M.,E. et al (2017) "A combined experimental atomic force microscopy-based nanoindentation and computational modeling approach to unravel the key contributors to the time-dependent mechanical behavior of single cells." Biomech Model Mechanobiol 16:297–311.

Friedl, P. Borgann, S. and Bröcker, E.,B. (2001) "Amoeboid leukocyte crawling through extracellular matrix: lessons from the Dictyostelium paradigm of cell movement." J. Leukoc. Biol. 70:491–509.

Iordan, A. Duperray, A. Gérard, A. Grichine, A. Verdier, C. (2010) "Breakdown of cell-collagen networks through collagen remodeling." Biorheology 47:277-295.

Iyer, P.,S. Mavoungou, L.,O. Ronzoni, F. et al (2018) "Autologous Cell Therapy Approach for Duchenne Muscular Dystrophy using PiggyBac Transposons and Mesoangioblasts." Mol Ther 26:1093–1108.

Mao, J. Duan, S. Song, A. et al (2012) "Macroporous and nanofibrous poly(lactide-co-glycolide)(50/50) scaffolds via phase separation combined with particle-leaching." Mater Sci Eng C 32:1407–1414.

Mihai, L.,A. Chin, L.,K. Janmey, P.,A. Goriely, A. (2015) "A comparison of hyperelastic constitutive models applicable to brain and fat tissues." J R Soc Interface 12:20150486-20150497.

Moeendarbary, E. Valon, L. Fritzsche, M. et al (2013) "The cytoplasm of living cells behaves as a poroelastic material." Nat Mater. 12:253-261.

Nicolle, S. and Palierne, J.,F. (2012) “On the efficiency of attachment methods of biological soft tissues in shear experiments.” J Mech Behav Biomed Mater 14:158–162.

Palade, L.,I. Verney, V. and Attané, P. (1996) “A modified fractional model to describe the entire viscoelastic behavior of polybutadienes from flow to glassy regime.” Rheol. Acta 35:265-273.

Perepelyuk, M. Chin, L. Cao, X. et al (2016) “Normal and fibrotic rat livers demonstrate shear strain softening and compression stiffening: A model for soft tissue mechanics.” PLoS One 11:1–18.

Plodinec, M. Loparic, M. Monnier, C.,A. et al (2012) “The nanomechanical signature of breast cancer.” Nat Nanotechnol. 7:757-765.

Pogoda, K. Chin, L. Georges, P.,C. et al (2014) “Compression stiffening of brain and its effect on mechanosensing by glioma cells.” New J Phys 16:075002.

Preziosi, L. Ambrosi, D. Verdier, C. (2010) “An elasto-visco-plastic model of cell agregates.” J. Theor. Biol. 262:35-47.

Puttini, S. Lekka, M. Dorchies, O.,M. et al (2009) “Gene-mediated restoration of normal myofiber elasticity in dystrophic muscles.” Mol Ther 17:19–25.

Qing, B. Canovic, E.,P. Mijailovic, A.,S. et al (2019) “Probing Mechanical Properties of Brain in a Tuberous Sclerosis Model of Autism.” J Biomech Eng 141:031001.

Shroff, S.,G. Saner, D.,R. Lal, R. (1995) “Dynamic micromechanical properties of cultured rat atrial myocytes measured by atomic force microscopy.” Am J Physiol Physiol 269:C286–C292.

Sneddon I.,N. (1965) “The Relation between Load and Penetration in the Axisymmetric Boussinesq Problem for a Punch of Arbitrary Profile.” Int. J. Engng Sci. 3:47–57.

Sollich, P. Lequeux, F. Hébraud, P. and Cates, M.,E. (1997) “Rheology of Soft Glassy Materials.” Phys. Rev. Lett. 78:2020-2023.

Storm, C. Pastore, J.,J. MacKintosh, F.,C. et al (2005) “Nonlinear elasticity in biological gels.” Nature 435:0–3.

Tan, K. Cheng, S. Jugé, L. Bilston, L.,E. (2013) “Characterising soft tissues under large amplitude oscillatory shear and combined loading.” J Biomech 46:1060–1066.

Tian, M. Li, Y. Liu, W. et al (2015) “The nanomechanical signature of liver cancer tissues and its molecular origin.” Nanoscale 7:12998–13010.

Vader, D. Kabla, A. Weitz, D. Mahadevan, L. (2009) “Strain-induced alignment in collagen gels.” PLoS One 4:e5902.

van Zwieten, R.,W. Puttini, S. Lekka, M. et al (2014) “Assessing dystrophies and other muscle diseases at the nanometer scale by atomic force microscopy.” Nanomedicine 9:393–406.

Verdier, C. Etienne, J. Duperray, A. Preziosi, L. (2009) “Review: Rheological properties of biological materials.” C. R. Physique, 10:790-811.

Zemła, J. Danilkiewicz, J. Orzechowska, B. et al (2018a) “Atomic force microscopy as a tool for assessing the cellular elasticity and adhesiveness to identify cancer cells and tissues.” Semin Cell Dev Biol 73:115–124.

Zemła, J. Stachura, T. Gross-Sondej, I. et al (2018b) “AFM-based nanomechanical characterization of bronchoscopic samples in asthma patients.” J Mol Recognit 31:e2752.